Signal processing technique for removal of NUBF induced error in spaceborne Doppler precipitation radar measurements

Simone Tanelli[a], Eastwood Im*[b], Luca Facheris**[a], Stephen L. Durden[b]

[a] Dipartimento di Elettronica e Telecomunicazioni, Università di Firenze, Firenze, Italy
[b] Jet Propulsion Laboratory, California Institute of Technology, Pasadena CA, USA

ABSTRACT

A sampling strategy and a signal processing technique are proposed to overcome Non Uniform Beam Filling (NUBF) errors on mean Doppler velocity measurements made by spaceborne weather radars. Effects of non uniformity of rainfall within the main antenna lobe in terms on the accuracy of standard estimators are first briefly shown, so as to point out that the bias introduced by NUBF on mean Doppler velocity estimates can be greater than the standard deviation of the estimated velocity, and that it depends on the along-track distribution of reflectivity. Then the sampling strategy is described, based on an oversampling of the integrated data in the along-track direction in order to retrieve information about the reflectivity pattern at the sub-beam scale. The proposed processing technique, named Combined Frequency-Time (CFT) technique, exploits the time series of spectra at fixed range to resolve the NUBF induced bias. The results and the evaluation of performances achievable by means of CFT, were obtained by applying a 3D spaceborne Doppler radar simulator to a 3D dataset of reflectivity and mean Doppler velocity measured through the NASA/JPL airborne Doppler radar ARMAR.

The radar system considered here is a nadir-looking, Ku band radar with a sufficiently wide antenna. It is shown how the error on mean Doppler velocity estimates can be reduced by means of CFT to the level predicted for such a radar system in the case of uniformly filled resolution volume (UBF).

Keywords: Spaceborne weather radar, Doppler, NUBF effects

1. INTRODUCTION

The Tropical Rainfall Monitoring Mission (TRMM)[1] has paved the way for the use of a spaceborne radar to measure precipitation. The Precipitation Radar aboard the TRMM satellite is a Ku band instrument with an antenna 3dB width of 0.71° resulting in an Instantaneous Field Of View (IFOV) of 4.3 km, a PRF (Pulse Repetition Frequency) of 2776 Hz and a range resolution of 250m. Its use, jointly with the TMI and VIRS passive sensors, has allowed important breakthrough in the understanding of the 3D structure of precipitating systems. Nonetheless, the Precipitation Radar lacks the capability of measuring the vertical motion of particles. As a consequence, the resulting precipitation classification into convective, stratiform and transitioning components provided by TRMM algorithms is sometimes ambiguous. More importantly, the estimate of vertical structure of latent heating (and therefore diabatic heating) must rely either on statistical-empirical schemes derived from nonhydrostatic cloud models, or incomplete physical schemes that are sensitive to inexact formulations of rain-ice mass fluxes derived from cloud model-generated hydrometeor profile structure functions. A common problem in both schemes is the large uncertainty in differentiating convective and stratiform precipitation, which in turn leads to errors in generating the vertical structures of heating.

For the above reasons, the utility of a spaceborne Doppler precipitation radar for gathering necessary information about physics and microphysics of atmospheric events has been recognized since the early 80's. Remarkable results were obtained in this context by airborne Doppler radars such as ARMAR[2], ELDORA[3], EDOP[4] and others. As a natural evolution to guarantee global coverage, the feasibility of acquiring Doppler measurements by spaceborne radars was investigated by various groups[5,6]. These studies mostly focused on Doppler measurements of uniform rain fields, following the assumptions successfully applied for the design of ground-based and airborne radars. Recent studies[7] have highlighted the negative impact of Non-Uniform Beam Filling (NUBF) on mean Doppler velocity measurements. In particular, it was

*Eastwood Im, Jet Propulsion Laboratory, M.S. 300-227 4800 Oak Grove Drive, Pasadena, CA 91109, U.S.A. E-mail: eastwood.im@jpl.nasa.gov **Luca Facheris, Dipartimento di Elettronica e Telecomunicazioni, Via di Santa Marta 3, 50139 Firenze Italy, E-mail:facheris@det.unifi.it

shown that the bias introduced by NUBF on mean Doppler velocity estimates (several m/s) can be greater than the standard deviation of the estimated velocity due to the weather signal fluctuations. Also it has been there highlighted how the shape of the expected power spectrum is affected by the horizontal reflectivity profile within the field of view. Therefore, such a bias affects almost equally every spectral moment estimation technique and cannot be reduced simply by changing the system parameters (other than by increasing the antenna size in order to reduce the NUBF factor). Finally, a signal processing approach aimed at reducing the NUBF effect on mean Doppler velocity estimates was introduced and some preliminary results shown.

In Section 2 of this paper the Doppler spectrum observed from a nadir looking radar is first described and the two standard spectral moment estimation techniques are recalled. Then, the dependence of mean Doppler estimation performances on different choices of system parameters is shown and the proposed configuration is discussed. In Section 3, after a brief overview of the problems induced by NUBF on the mean Doppler estimation, the refined version of the signal processing technique - referred to as Combined Frequency-Time (CFT) - devised to minimize NUBF induced errors on mean Doppler velocity estimates is described. CFT is a time-frequency spectral analysis technique by which sequences of Doppler spectra pertinent to radar volumes that are partially overlapped in the along-track direction are processed to get more detailed information about the along-track profile of reflectivity within the IFOV and consequently correct for the correlated NUBF induced bias. The results and the evaluation of performances achievable by means of CFT were obtained by applying a 3D spaceborne Doppler radar simulator to a 3D dataset of reflectivity and mean Doppler velocity measured through the NASA/JPL Airborne Rain Mapping Radar (ARMAR).

2. RAINFALL DOPPLER SPECTRUM MEASUREMENTS FROM SPACE

Given a point scatterer moving with velocity $v = [v_x, v_y, v_z]$ (positive v_z corresponding to falling particles), the radial velocity observed by a nadir looking radar orbiting at altitude h_S with velocity v_S is given by:

$$v_r = (v_x - v_s)\cdot \sin\theta\cos\phi + v_y \cdot \sin\theta\sin\phi + v_z \cdot \cos\theta \tag{1}$$

where θ and ϕ are respectively the elevation and azimuth angles in the antenna coordinate system. For any low earth orbiting satellite $v_S \cong 7$ km/s. This is about 3 orders of magnitude higher than the typical rainfall velocities therefore the first term of Eq. (1) dominates even for a small radar beamwidth θ_{3dB} (θ_{3dB} is defined as the one-way beamwidth hereinafter). Furthermore, the surfaces at constant Doppler shift (isodops) are given by the family of cones with vertices at the spacecraft and generating axes along x. Since for most spaceborne precipitation radar designs[1,6] θ_{3dB} is less than 1°, the isodops within the main lobe can be well approximated by a family of planes. Moreover, for a nadir looking radar, the isodops are orthogonal to x, so that the radial velocity v_r of a target at distance $r \cong h_S$, can be well approximated as:

$$v_r = -(v_s / h_s)x + v_z \tag{2}$$

Since it is generated by different relative raindrop speeds within the radar antenna beamwidth, the power spectrum is:

$$P(f;\mathbf{r}_V) = \int_{r_1}^{r_2}\int_0^{\pi}\int_0^{2\pi} \eta[\mathbf{r}, f - f'(\theta,\phi)]W(\mathbf{r},\mathbf{r}_V)\, r\sin\theta\, d\theta\, d\phi\, dr \tag{3}$$

where r_1 , r_2 are the range limits of the resolution volume centered at $\mathbf{r}_V$, $\eta(r,f)$ is the natural Doppler velocity spectrum associated with the distribution of the falling particles, f' is the Doppler shift, and $W(r;r_V)$ is a weighting factor:

$$W(r;r_V) = \frac{C\cdot G_a^2(\theta,\phi)\cdot |G_r(r-r_V)|^2}{L(r)\cdot r^4} \tag{4}$$

where C is the radar constant, G_a is the antenna gain pattern, G_r is the range weighting function, and L is the two-way atmospheric attenuation. From Eq. (2), f' can be approximated as:

$$f'(\theta,\phi) = qx \tag{5}$$

$$q = \frac{2v_s}{\lambda h_s} \tag{5'}$$

where λ is the radar wavelength.

The shape of $\eta(r,f)$ is affected by turbulence and wind shear, and by the fall speed of the hydrometeors[8]. Typically, wind shear and turbulence combined contribute between 1 and 5 m/s to the spectral width[6]. The average terminal fall speed is typically in the 2 to 8 m/s range in the absence of up- or down-drafts[8,9], and it can be approximated by a Gaussian spectrum with an average vertical rainfall velocity v_R and a spectral width that is close to 1 m/s. The resulting natural Doppler spectral width σ_R, therefore, varies between 2 and 5 m/s.

Assuming a nadir-pointing radar with a circularly symmetric antenna pattern is observing a uniform rain field (i.e. $\eta(r,f) = \eta(f)$ hereon referred to as UBF condition), the total backscatter signal spectrum can be approximated by a Gaussian centered at $f_R = -2v_R/\lambda$. The corresponding frequency spectral width σ_U can be estimated as[5]:

$$\sigma_U = \frac{2}{\lambda}\sqrt{\sigma_R^2 + \frac{\theta_{3dB}^2 v_S^2}{16\ln(2)}} \tag{6}$$

The parameter $\sigma_{UN} = \sigma_U/PRF$ (PRF: radar Pulse Repetition Frequency) is commonly adopted to quantify how good the average rainfall Doppler velocity in a given radar resolution cell can be estimated by means of spectral moments estimators such as the autocovariance analysis by means of Pulse Pair (PP) processing technique and the spectral analysis by means of Discrete Fourier Transform (DFT) [10]. They both estimate the mean Doppler velocity of rainfall from a finite sequence of M complex radar samples $\{\tilde{s}_n\}$ spaced by $T_S=1/PRF$ and affected by signal fluctuation[11] and noise:

The PP technique estimates the mean Doppler velocity $\hat{v}^{PP}$ through one-lag correlation of $\{\tilde{s}_n\}$:

$$\hat{v}^{PP} = -\frac{\lambda}{2}\frac{1}{2\pi T_S} arg\left(\frac{1}{M-1}\sum_{n=-(M-1)/2}^{(M-1)/2-1}\tilde{s}_n^*\tilde{s}_{n+1}\right) \tag{7}$$

Eq. (17) assumes that the pulses are evenly spaced. Unevenly spaced pulse pair techniques have also been proposed to reduce range ambiguities on velocity estimates [10,12]. This estimator is unbiased if the spectrum is symmetric with respect to the mean velocity, and its performances are almost at the Cramer-Rao bound for $\sigma_{UN} < 0.05$, on the other hand the variance of estimates increases exponentially with σ_{UN}.

The mean velocity estimate through DFT technique can be expressed as:

$$\hat{v}^{DFT} = -\frac{\lambda}{2MT_S}\left\{\hat{m}' + \frac{1}{(S_P+S_N)-\hat{S}_N}\sum_{m=\hat{m}'-M/2}^{\hat{m}'+M/2}(m-\hat{m}')\cdot\left[(P_{\mathrm{mod}_M(m)} + N_{\mathrm{mod}_M(m)}) - \hat{N}_{\mathrm{mod}_M(m)}\right]\right\} \tag{8}$$

where S_P and S_N are the signal and (stationary) noise power, respectively, while $\hat{S}_N$ is the estimated mean noise power and $\hat{m}'$ is an index corresponding to an approximation of the mean spectral frequency. The discrete spectra P_i and N_i are sampled at $f=i/MT_S$..

An important issue pertinent to the use of this technique is the approach to determine the initial guess index $\hat{m}'$. When the Doppler spectrum is narrow (e.g., $\sigma_{UN} < 0.1$) and M is large (e.g., $M>1000$), $\hat{m}'$ in Eq. (8) can be chosen equal to the index of the sample with the largest power [10]. That is, $\hat{m}': \tilde{P}_{\hat{m}'} = \max\{\tilde{P}_k\}$ for $k=0,...,M-1$. For the spaceborne radar configuration in this study, however, neither of these conditions applies. In fact, for what concerns σ_{UN}, a maximum PRF is imposed by the thickness of the precipitating layer (roughly up to 20 km), therefore a maximum PRF of 7500 Hz can be adopted in order to have a large enough maximum unambiguous range. On the other hand, an upper limit on the antenna diameter D (roughly of 5m) is set by economical/technological constraints. Hence, the minimum achievable σ_{UN} would be > 0.1. Also the integration time $T_I = M\,T_S$ undergoes more stringent limitations than it would in the case of ground-based or airborne systems, due to the high antenna velocity (which sets issues of stationarity of the observed process[7] and of scanning strategy). Therefore, a two-step DFT approach was devised which provides more stable estimates. In the first step, Eq. (8) is applied with $\hat{m}' = 0$ and the first velocity guess $\hat{v}^{(1)}$ is obtained. In the second step, $\hat{m}'$ is set equal to $\hat{v}^{(1)}/(-\lambda/2MT_S)$.

The DFT technique is affected by spectral aliasing (in terms of both variance and bias on estimates) and is less computationally efficient than PP. On the other hand, it is less sensitive to σ_{UN} than PP and is not affected by asymmetry of the spectrum.

The performance of standard spectral moments estimators based on the UBF condition have been studied extensively and used successfully in the design of many airborne Doppler radar systems, such as ARMAR[2], ELDORA[3], EDOP[4] and others. These systems were designed for narrow Doppler spectra (e.g., $\sigma_{UN} = 0.1$ for ARMAR, $\sigma_{UN} = 0.05$ for EDOP and $\sigma_{UN} = 0.04$ for ELDORA) in order to provide high velocity measurement accuracy. For example, with the chosen radar parameters EDOP can achieve a Doppler velocity measurement accuracy approaching 0.1 m/s [4], which is far better than the requirement for most current science studies and applications.

While a spaceborne Doppler radar can exploit a larger antenna to reduce θ_{3dB}, the orbital speed v_s is more than one order of magnitude higher, thus broader Doppler spectra are expected. However, the scientific requirement for global measurements of rainfall vertical velocity is 1 m/s: Fig. 1 shows that a spaceborne system with the parameters of Table 1 can achieve such an accuracy under the UBF condition. Notice that the performances of both estimators degrade significantly when $|v_R|$ approaches the Nyquist limit $v_m = PRF\ \lambda/4$ (this happens only in presence of remarkable up- or down-drafts for the considered configuration).

In general, under UBF conditions, spaceborne radars can estimate rainfall's vertical velocity with negligible biases and with standard deviations ranging between 0.5 and a few meters per second. With a well-designed system that provides sufficient spectral sampling and number of samples, the standard deviation can be reduced to less than 1 m/s, necessary for most science applications. Also, when $\sigma_{UN} > 0.1$ (which, for PRF = 6000 Hz, corresponds roughly to an along-track antenna size $D < 10m$), the standard deviation of the DFT estimates is smaller than that of the PP estimates[7], hence requiring a smaller number of samples M. Notice however that PP estimates are always unbiased, while DFT ones exhibit an increasing bias when SNR drops below $10\ dB$ and $|v_R|$ approaches v_m.

Clearly, the ~2 km IFOV resulting from the parameters in Table 1 allows to apply Eq. (6) only under the hypothesis of an horizontally uniform rain field, which can be a valid assumption for widespread stratiform rain, but does not hold for convective rain systems and severe storms[13]. When NUBF occurs, the variability of $\eta(r,f)$ within the radar cell weights differently the Doppler frequency shifts due to v_S, so that the measured spectrum undergoes shape distortions, and the accuracy on vertical rainfall velocity v_R estimates is degraded. Since isodops are orthogonal to the along-track direction, only the NUBF in the along track direction will affect the shape of the power spectrum. In order to emphasize the along-track

v_s	7 km/s
h_s	432 km
PRF	6000 Hz
F_c	13.6 GHz
θ_{3dB}	0.3°
D	5 m
M	64-128-256

Table 1. Spaceborne radar system parameters: adopted configuration

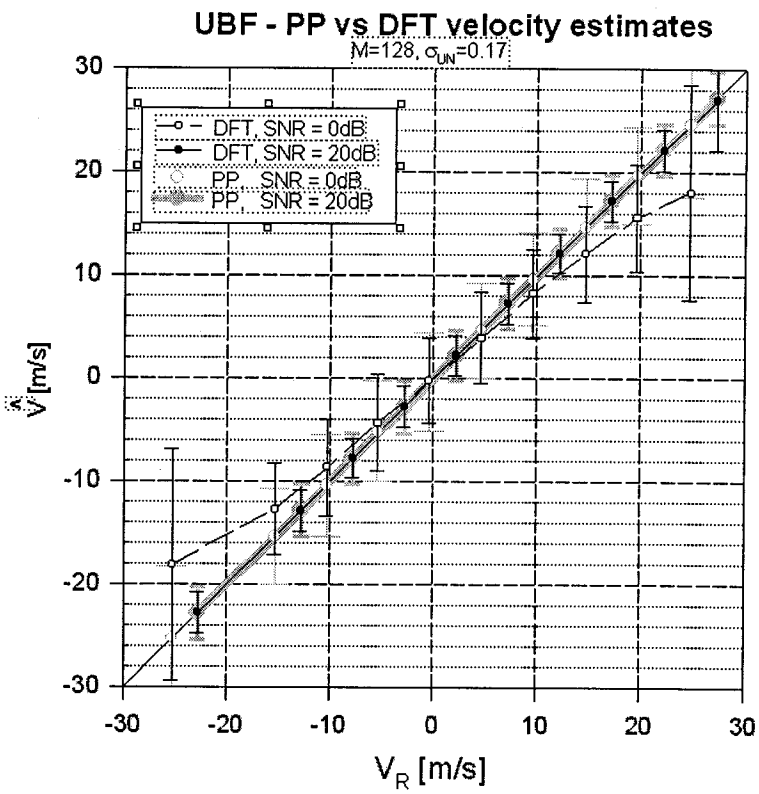

Figure 1 Mean value (indicated by circles and lines, see legend) and confidence intervals (error bars indicate the $\pm 2\sigma$ interval) of the PP and DFT velocity estimators versus true rainfall vertical velocity v_R for two different values of signal to noise ratio at the radar receiver, when UBF conditions apply. Notice that the maximum unambiguous velocity for the adopted configuration is 33 m/s.

dependency of the Doppler shift introduced by the satellite motion, we decompose the weighting function as $W(r) = W_{YZ}(y,z)\cdot W_X(x)$ and re-formulate Eq. (3) as:

$$P(f;r_v) = \int_{-\infty}^{\infty} \eta_X(x', f - qx')W_X(x)dx \tag{9}$$

$\eta_X(x,f)$ in Eq. (7) is obtained by integrating $\eta(r,f)\cdot W_{YZ}(y,z)$ in the cross-track plane (i.e., the y-z plane).

It has been found [7, 14] that NUBF causes a significant bias on estimates, independently of the estimation technique and of the choice of M or SNR. The NUBF induced bias depends only on the shape of the along track reflectivity profile $Z_x(x,z_n) = \int \eta_X(x,f)df$ within a radar resolution cell at altitude z_n. The magnitude of such a bias can be of several m/s, hence seriously affecting vertical velocity estimates made through spaceborne radars. This is particularly evident in Fig. 2 where spaceborne Doppler measurements were simulated[7] over a high resolution 3D dataset obtained from NASA/JPL ARMAR radar during the KWAJEX campaign on Sept. 2nd 1999. The event was heavily convective, exhibiting significant

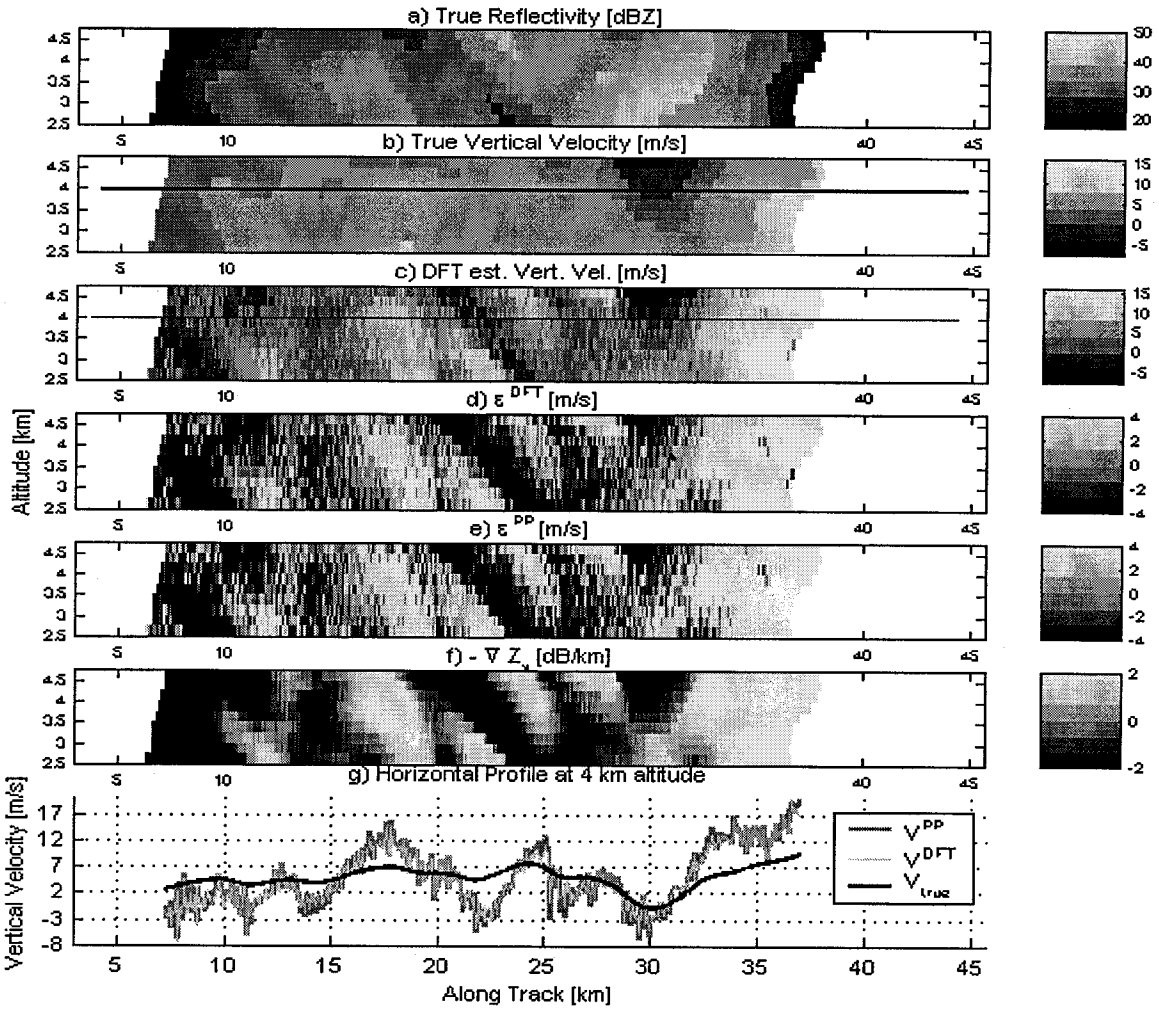

Figure 2 Event A245 - Vertical sections of precipitation in the along track direction. From top to bottom: a) true reflectivity; b) true vertical velocity; c) $\hat{v}^{DFT}$; d) error on $\hat{v}^{DFT}$; e) error on $\hat{v}^{PP}$; f) reflectivity gradient (sign reversed) in the along track direction; g) one sample of horizontal profile of vertical velocity at 4km altitude (indicated by the horizontal lines in plots b) and c)). Notice that the middle band of gray tones refers to the -1.33÷+1.33 m/s range in plots d-e, that is the 'acceptable' error range.

updrafts and sharp variations of rainfall at the small scale (see Figs. 2a, 2b and 2f) and it will be referred to as A245.

Fig 2c shows the $\hat{v}^{DFT}$ fields obtained with M=64, and Fig. 2d shows the corresponding error fields $\varepsilon^{DFT} = \hat{v}^{DFT} - v_R$. The corresponding $\hat{v}^{PP}$ are practically identical and thus only the error fields $\varepsilon^{PP} = \hat{v}^{PP} - v_R$ are reported in Fig. 2e for comparison with DFT estimates. Fig. 2f shows the reflectivity gradient in the along track direction $\nabla Z_x(x,z) = d[Z_x(x,z)]_{dBZ}/dx$ in dBZ/km.

Notice first that, since consecutive spectra refer to overlapping resolution volumes (in fact each spectrum is calculated every $\Delta_x = 75m$), the NUBF effect is highly correlated in the along-track direction. On the contrary, the error due to weather signal fluctuations is totally uncorrelated since T_I is much larger than the echo decorrelation time (which is approximately the inverse of the rainfall Doppler bandwidth).

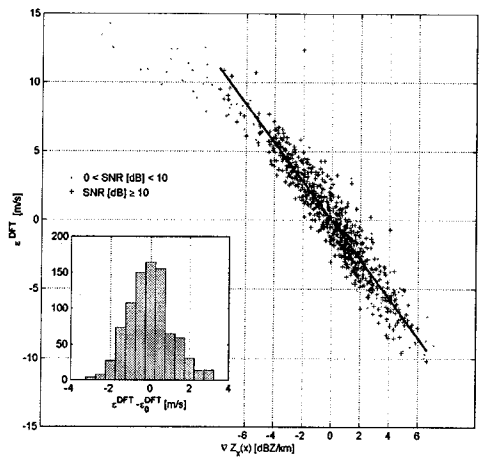

Figure 3 - Event A245 - $\hat{v}^{DFT}$ vs. reflectivity gradient in the along track direction. Grey dots refer to cells with SNR < 10dB, plus signs to cells with SNR > 10dB. The regression line was calculated for the latter case. The histogram on the left shows the residual error with respect to the regression

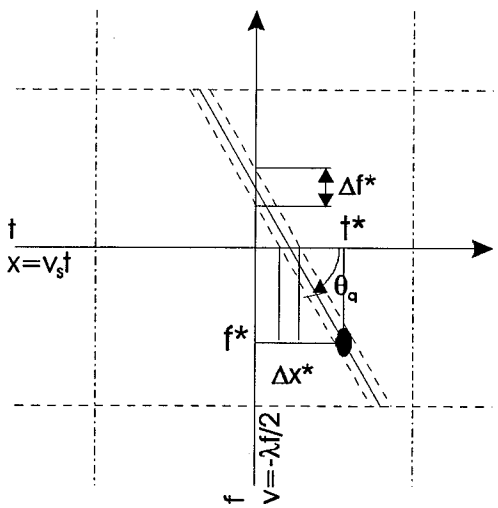

Figure 4 Frequency-time signature of a rainfall target

Also from visual inspection, Fig. 2 highlights the high correlation between ε^{DFT} and ε^{PP}. Furthermore, both errors show a correlation coefficient of ≈0.82 with $-\nabla Z_x$.

Fig 3 shows that the error contribution from NUBF is absolutely dominant. The regression line $\varepsilon_0 = \alpha - \beta \nabla Z_x$ for DFT estimates with SNR > 10dB is plotted. The slope coefficient β=1.42 and the residual error $\varepsilon^{DFT} - \varepsilon_0$ is below 1 m/s in 66% of cases as shown in the histogram in the figure. The value of β was calculated also for several datasets relative to atmospheric events of different kind, and it was found to vary only by less than 20%. This small sensitivity to the nature of the event, and the fact that the residual error is independent of NUBF led to the development of adequate algorithms for NUBF-induced bias reduction.

3. RETRIEVING THE MEAN VERTICAL VELOCITY OF RAINFALL THROUGH ALONG TRACK OVERSAMPLING: THE CFT TECHNIQUE

Since the mean velocity of each ensemble of scatterers in the radar resolution volume, though unknown, can be considered constant during the time it is illuminated by the radar (less than 0.5 s for the case considered), the relative position of each ensemble can be retrieved in principle from a sequence of estimated Doppler spectra, each computed on M echoes. Evidently, errors may arise due to the fact that ensembles of scatterers with different values of σ_R have different spatial extent $\sigma_R h_s/v_s$ in the frequency-time plane and may overlap. Also, ambiguity can occur between two ensembles of scatterers when $v_R^{(1)} - qx^{(1)} = v_R^{(2)} - qx^{(2)}$ where $v_R^{(i)}$ and $x^{(i)}$ are the average vertical velocity and along track position of the i-th ensemble of scatterers, respectively. Although this possibility can be considered unlikely , it is taken into account in the following.

The need for information about the rainfall patterns at a sub-beam scale brings to issues that are common with the SAR theory: in particular it is of paramount importance to solve simultaneously the velocity and the position (at sub

beam scale) of the observed targets. Let us consider a nadir looking Doppler weather radar: range resolution Δr and cross-track resolution Δy are defined respectively by the input receiver filter and by the antenna beamwidth along y, while the along track resolution Δx can be achieved by means of a spectral processing approach that can be first described by analogy with the Doppler beam sharpening approach[15]. Fig. 4, reporting the time of flight (position) in the abscissa and the Doppler frequency (velocity) in the ordinate, shows that to achieve a given resolution Δ_x, a spectral resolution of $\Delta f = q\Delta_x$ is needed at the receiver, with $q=2v_s/\lambda h_s$. In the case of rainfall targets, evidently the spectral resolution Δf should not exceed the natural spectrum width $\Delta f^*=(2/\lambda)\sigma_R$. Therefore, the maximum resolution useful for identifying and tracking rainfall echo contributions would be $\Delta f^*=4\sigma_R/\lambda$. For instance, if σ_R=3 m/s, then Δf^* = 570 Hz, and the required along track resolution would be $\Delta x^* = 370\ m$ that corresponds to impose $M < 320$. Still referring to Fig. 4, it is evident that a good time-frequency tracking of echoes requires that the spectral resolution be at least equal to frequency shift that the target undergoes in the pulse integration time $T_I = MT_s$. The corresponding along-track resolution is therefore:

$$\Delta_x^{(U)} = \sqrt{h_S\,\lambda/2} \tag{10}$$

that for the given system corresponds to less than 70 m, which is smaller than Δ_x^* even for for $\sigma_R = 0.5$ (which can be considered as an absolute lower limit for a rainfall target). Therefore, M = 60 was determined as the optimum value for the adopted configuration, and simulations were performed with 3 different values of M: 64 for the optimum (enabling FFT processing), 32 for coarser spectral resolution and redundant spatial resolution, and 128 for finer spectral resolution and coarser spatial resolution. Notice that for M = 128, when significant NUBF is present, the observed process cannot be considered stationary: for this reason, a simulated spectrum was approximated by combining spectra calculated at sub-intervals of time during which the hypothesis of stationarity is valid.

3.1 Combined Frequency-Time technique for mean Doppler estimation

The rainfall field within the radar volume of resolution can be seen as the superposition of a uniform rainfall field R_{UF} and a of an independent rainfall intensity pattern $R_{NF}(r)$ with features at a scale smaller or comparable to the IFOV. In the following their associated natural Doppler spectra $\eta_{UF}(f)$ and $\eta_{NF}(r,f)$ respectively.

Assuming that the center coordinates of a radar resolution volume are $x_V(t)=v_S t$ $y_V(t) = y_V$ and $z_V(t) = z_V$, we can rearrange Eq (9) to obtain the following time-frequency representation of the Doppler frequency spectrum associated with a constant altitude section of the rainfall field:

$$\begin{aligned} P(f,t) &= \eta_{UF}(f) + P_{NF}(f,t) \\ P_{NF}(f,t) &= \int_{-\infty}^{\infty} \eta_{NF}(x, f - q(x - v_S t))\, W_X(x - v_S t)\, dx \end{aligned} \tag{11}$$

where:

$$W(\boldsymbol{r}, \boldsymbol{r}_V(t)) = W_{YZ}(y - y_V, z - z_V) \cdot W_X(x - v_S t) \tag{12}$$

and $\eta_{NF}(r,f)$ is the integral in the cross track plane of $\eta_{NF}(r,f)$ $W_{YZ}(y\text{-}y_V, z\text{-}z_V)$. Let us now define the target track in $P_{NF}(f,t)$ as:

$$\begin{aligned} P_\tau(\beta) &= P_{NF}(-q v_S \beta, \beta + \tau) = \\ &= \int_{-\infty}^{\infty} \eta_{NF}(x, -q(x + v_S \beta))\, W_X(x - v_S(\beta + \tau))\, dx \end{aligned} \tag{13}$$

Since the η_{NF} term in the integral does not depend on f, for any given value of β $P_\tau(\beta)$ is given by the contributions of the ensemble of scatterers having all the same radial velocity with respect to the radar at any instant around τ. If the along-track extension of the ensemble of scatterers is smaller than Δx (that is it can be considered 'concentrated' in one point), the resulting track $P_\tau(\beta)$ is a Gaussian with width directly dependent on the system parameters (i.e., $\propto h_S\, \theta_{3dB} / q$). On the other hand, if the ensemble of scatterers is significantly spread out in the along track direction, the width of $P_\tau(\beta)$ is larger than that predicted value.

Notice also that the integral:

$$I(\tau) = \int_{-\infty}^{\infty} P_\tau(\beta) d\beta \tag{14}$$

corresponds to the total power contribution of the aforementioned ensemble of scatterers. Adopting the Radon Transform terminology, $I(\tau)$ is the front projection of $P_{NF}(f,t)$ along the direction given by the Doppler shift rate vs time coefficient (qv_S).

The CFT is based on the calculation of $P_\tau(\beta)$ at $\tau = kT_P$ where $T_P = \min\{\Delta x / v_S \; ; \; \Delta f / (qv_S)\}$ The target center $\tilde{t}_\gamma$ and $\tilde{f}_\gamma$ associated with each $P_\tau(\beta)$ are determined by finding the maximum of the antenna pattern that best fits $P_\tau(\beta)$. The Gaussian fit is adopted consistently with the assumptions on the antenna pattern and in order to reduce the effects of noise (in particular speckle noise). The target center is then associated with the features in the x-v plane:

$$\begin{aligned} \tilde{x}_\tau &= v_S \tilde{t}_\tau \\ \tilde{v}_\tau &= -\frac{2}{\lambda} \tilde{f}_\tau \end{aligned} \tag{15}$$

The total reflectivity of the target is also stored:

$$\tilde{z}_\tau = I(\tau) \cdot qv_S \tag{16}$$

Targets are finally interpolated in order to obtain an along-track profile of mean Doppler velocity $v_X(x)$ with constant spatial resolution. Interpolation is weighted by their respective total power estimates $\tilde{z}_\tau$, and by the functional $E_G(i)$ proportional to the relative root mean square of the track $P_\tau(\beta)$ versus the Gaussian with predetermined width:

$$v_X(x) = \sum_i \tilde{v}_i \cdot \tilde{z}_i \cdot E_G(i) \cdot W_X(x - \tilde{x}_i) \tag{17}$$

The weighting factor E_G is used to assess and remove the possible ambiguity discussed at the beginning of this section: if the ensemble of scatteres showing the same relative velocity is actually spread over a distance larger than Δx, the shape of its track $P_\tau(\beta)$ is broader than the expected value (see Eq. (13)). Although correction is theoretically possible by deconvolving $W_X(x)$ from $P_\tau(\beta)$ this kind of (computationally heavy) processing would require a very high number of samples and simulations showed little or no benefit for the configuration discussed here. On the other hand, the use of the functional E_G simply reduces the weight of estimates that are likely to be affected by this kind of ambiguity. Since the ambiguity occurs when $dv_R(x)/dx = v_S/h_S \cong 16.2 \; m\,s^{-1}\,km^{-1}$, this can be true only for very short intervals. Therefore more reliable estimates (within the antenna footprint) compensate through Eq. (17) the local unreliable estimate.

Since a Doppler spectrum is estimated separately at every range bin, a spectra stack $\underline{\underline{P}}(n,k,h)$ can be defined, where the element $P_{n,k,h}$ is the Doppler spectrum line at $f=(n-M/2)/T_I$, gathered at time $T_k = k\,N\,T_I$ and at the range bin h. Notice that $N = 1$ when a continuous stream of pulses is processed as in a nadir only operating mode, instead, N > 1 is used to introduce gaps in the sequence (e.g., when a radar cross-track scanning capability is simulated).

CFT processes separately every sequence of spectra at a constant range. The number of spectra involved in the calculation of $P_\tau(\beta)$ is given by:

$$M_x = \frac{1}{q} \frac{1}{v_S T_S^2} \frac{1}{NM} \tag{18}$$

Therefore the number of points M_B where $P_\tau(\beta)$ is calculated is the smaller between M and M_x . When $\Delta f = q\Delta x$ (i.e., the along track resolution is given by Eq. (10)), the last equation becomes $M_x = M$ which leads to the maximum value of M_B . Different choices of M will lead to smaller M_B (larger variance on $\tilde{t}_\tau$ and $\tilde{f}_\tau$ estimates) but also smaller values of T_P, that is , a larger number of independent estimates is calculated which are finally weight averaged in Eq. (17). Notice also that the filtering action of Eq. (17) is more pronounced when small M and N are used. The overall sensitivity CFT accuracy on the choice of M is briefly discussed in the following analysis of the simulations results.

4. RESULTS

The results shown in the following refer to the dataset of Fig. 2 and discussed in Section 2. Simulations were carried out for the 6 different sampling modes indicated in Table 2. In simulations A,B and C the continuous stream of pulses is processed with different choices of M, that simply modify Δx ($=v_S T_I$) and Δf ($=PRF/M$). In simulation 2B each spectrum is obtained by processing 64 samples, while spectra are calculated every 32 pulse transmissions (i.e., spectra are calculated on overlapping sequences of samples). Instead , in simulations B2 and B4 spectra are still calculated on 64 samples but with a larger Δx, since a number of consecutive echoes (M and $3M$, respectively) are not exploited. This kind of simulation is justified by the need of assessing the performances of the spaceborne Doppler radar when operating in cross-track scanning mode (thus simulations B2 and B4 refer to a 2 and 4 beam system, respectively).

Fig. 5 shows the CFT estimated vertical velocity field along with the corresponding errors for simulations A B and C. Notice that the grayscale for the vertical velocities (true and estimated) and that of the errors are consistent with those of Fig. 2 where the estimates obtained through PP and DFT are shown. It is evident that CFT is able to eliminate the NUBF induced bias, and the major features of the convective event are correctly estimated both in magnitude and position. The residual error is mainly dependent on SNR and totally uncorrelated with ∇Z_x.

In order to further analyze CFT performance, Table 3 reports the root mean square error (rms) for all 6 sampling modes and different SNR ranges along with the corresponding values for DFT estimates. Notice that CFT estimates calculated when SNR > 10dB show almost constant rms among A,B and C confirming the effectiveness of the weighted averaging of neighboring estimates through Eq. (17) and showing significant robustness of CFT to the choice of M. The calculated rms are significantly smaller than the expected performance of the DFT estimator under UBF conditions because of the filtering action of Eq. (17). Notice that no improvement for standard estimators could be achieved in NUBF conditions by filtering since most of the error is not due to the signal fluctuations but to the NUBF induced deformation of the expected power spectrum (this is evidenced also in Table 3 by the fact that the rms of DFT estimates in NUBF conditions are roughly doubled with respect to the UBF condition).

The rms values of CFT estimates for lower SNR are somewhat conditioned by the large errors that can be observed at the edges of the precipitating area. These local errors are more pronounced for smaller M since in that case the low SNR combines with the absence of data on one side and therefore Eq. (17) cannot effectively compensate for the local lack of reliable estimates.

Results from simulations 2B, B2 and B4 show that the rms varies consistently with the increase/decrease of Δx only at high SNR. The reverse tendency at low SNR is mainly due to the spatial filtering of Eq. (17) which can occasionally overweight a neighboring estimate obtained at high SNR and therefore bias towards that value the local estimate obtained at low SNR.

The effectiveness of the spatial filtering towards the removal of the 'spreaded scatterers' ambiguity is evident around km 32 between 3.5 and 4 km altitude: at the front edge of the updraft (negative velocities indicate rising particles) the vertical velocity gradient reaches the value of 16 m/s km^{-1} and large errors in CFT estimates would occur without the use of the functional E_G. Instead, the calculated errors in that area fall within the normal rms range due to signal fluctuation.

Mode	M	N ($\Delta x = N T_I$)
A	32	1
B	64	1
C	128	1
2B	64	0.5
B2	64	2
B4	64	4

Table 2. Simulations parameters. N ≤ 1 can be assumed for a nadir only operating radar.

SNR (dB)	CFT						DFT						DFT UBF M=64
	A	B	C	2B	B2	B4	A	B	C	2B	B2	B4	
>0	1.92	1.65	1.12	1.72	1.28	1.29	4.60	4.33	4.13	4.32	4.33	4.35	--
0÷5	5.67	4.74	3.12	5.65	3.00	2.24	6.62	6.13	5.75	6.30	6.20	6.44	2.8÷1.9
5÷10	3.39	3.07	1.26	2.16	2.09	1.90	7.52	7.44	7.24	7.46	7.46	7.39	1.9÷1.6
10÷20	0.88	0.77	0.77	0.64	0.94	1.14	4.37	4.11	3.93	4.05	4.10	4.13	1.6÷1.4
>20	0.57	0.58	0.58	0.47	0.75	0.98	3.14	2.81	2.58	2.80	2.81	2.70	<1.4

Table 3. Root mean square errors (m/s) on vertical velocity estimates through CFT and DFT for different scanning strategies and different SNR ranges. The column at the right shows the expected range of rms for the DFT estimator in UBF conditions and M = 64.

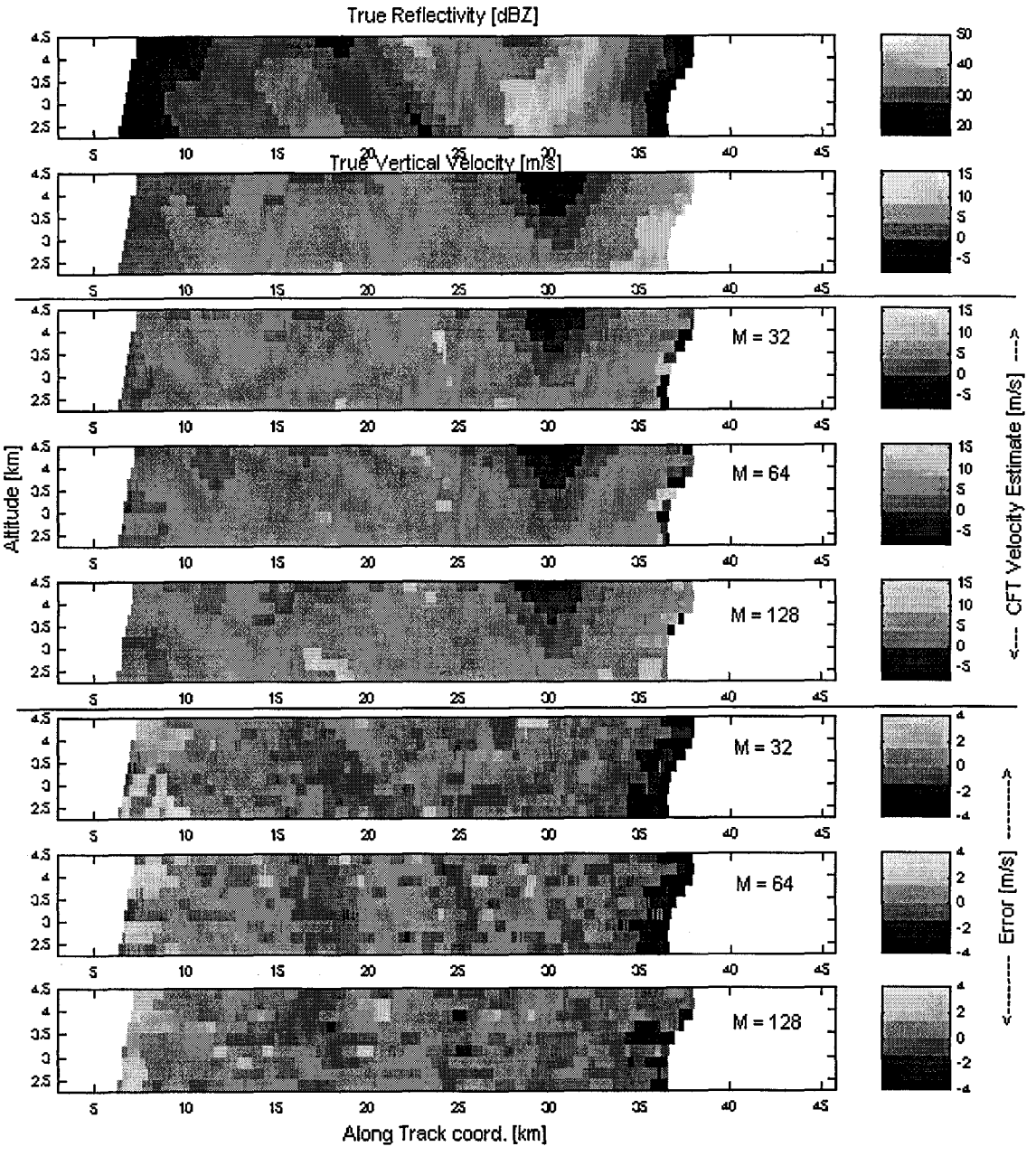

Figure 5. Event A245 - Sept. 2nd 1999 – Vertical sections of the event. From top to bottom: true reflectivity field; true vertical velocity field; CFT estimates for simulation modes A, B, C; velocity error fields for the same modes. The middle band of gray tones refers to the -1.33÷+1.33 m/s range in the error plots, that is the 'acceptable' error range. In the vertical velocity plots, the same middle tones band refers to the 0÷8 m/s range, which indicates roughly the rainfall droplets terminal velocity range. The dark area in vertical velocity plots around km 30 is an updraft well reconstructed by CFT in all modes. Instead, the light area at the trailing edge of the system is a downdraft which is detected only by mode C (M=128) due to the extremely low local SNR and the position at the edge of available data. On the other hand, modes with smaller M provide better reconstruction of features of vertical velocity field within the precipitating area (e.g., around km 18 and 22).

5. CONCLUSIONS

When a homogeneous rainfield is observed, a spaceborne Doppler rain radar can provide good estimates of mean vertical velocity of rainfall by means of standard spectral moment estimation techniques: 1 m/s accuracy is a goal easily achievable. However, this possibility is evidently too much related to the size of the antenna footprint and on the characteristics of the observed atmospheric event. This consideration, along with work done by researchers in the field of spaceborne weather Doppler radar, led us to investigate the performances of a Ku band radar with a 5m antenna, and to develop a novel algorithm to remove NUBF effects on mean Doppler velocity estimation, since when the rain field is not homogeneous within the volume of resolution, such spectral techniques are heavily affected by bias. This is strictly related to the along-track profile of rainfall, and cannot be limited by simply changing the spectral processing parameters (such as *PRF* and *M*) or the estimation technique since NUBF modifies the expected power spectrum. This is confirmed by the highly correlated errors of the spectral moment estimators, and by their observed dependence on the along track profile of reflectivity. The result is that even for IFOVs as small as that considered in this paper (2.2 km), NUBF induced bias can deteriorate the accuracy of estimates by several m/s.

The proposed Combined Frequency-Time technique follows an approach close to the beam sharpening method, and processes series of spectra gathered on volumes of resolution partially overlapping in the along-track direction in order to remove the NUBF induced bias. Although several details in the signal processing algorithm should be changed accordingly to the specific system configuration adopted, the main concept holds for a wide variety of spaceborne system configurations. In particular, the results for a specific configuration discussed in this work proved that:

1) The CFT approach can effectively remove the NUBF induced bias on mean Doppler velocity estimates, and the required accuracy of 1 m/s can be easily achieved for SNR > 10dB.

2) When a nadir only radar is used, the CFT technique is robust to changes in the number of samples used to calculate each spectrum.

3) When a cross-track scanning strategy is adopted, the loss of some samples in the along-track direction decreases the accuracy of estimates as expected, but the desired 1 m/s accuracy can still be achieved at SNR > 10 dB.

In depth analysis of the results showed the importance of a correct definition of the method for the final averaging of irregularly spaced estimates and some further attention will be dedicated to this aspect in order to improve the performances of the technique in extreme conditions (low SNR and partial lack of signal from the neighboring areas).

6. ACKNOWLEDGEMENT

The research described in this paper was performed at the Jet Propulsion Laboratory, California Institute of Technology, under contract with the National Aeronautics and Space Administration, and with the cooperation of University of Firenze through a program funded by ASI (Italian Space Agency).

REFERENCES

1. C. Kummerow, J. Simpson, O. Thiele, W. Barnes, A.T.C. Chang, E. Stocker, R.F. Adler, A. Hou, R. Kakar, E. Wentz, P. Ashcroft, T. Kouz, Y. Hong, K. Okamoto, T. Iguchi, H. Kuroiwa, E. Im, Z. Haddad, G. Huffman, B. Ferrier, W.S. Olson, E. Zipser, E.A. Smith, T.T. Wilheit, G. North, T. Krishnamurti, and K. Nakamura, 2000: The status of the Tropical Rainfall Measuring Mission (TRMM) after 2 years in orbit. *J. Appl. Meteor.*, 39, pp.1965-1982.

2 S.L. Durden, E. Im, F.K. Li, W. Ricketts, A. Tanner and W. Wilson, 1994: ARMAR: An Airborne Rain-Mapping Radar. J. Atmos. Oceanic Technol., 11, pp. 727-737.

3 P.H. Hildebrand, C.A. Walther, C.L. Frush, J. Testud and F. Baudin, 1993: The ELDORA/ASTRAIA Airborne Doppler Weather Radar: Goals, Design, and First Field Tests. Proceedings of IEEE, 82, pp. 1873-1990.

4 G.M. Heymsfield, S.W. Bidwell, I.J. Caylor, S. Ameen, S. Nicholson, W. Boncyk, L. Miller, D. Vandemark, P.E.

Racette and L.R. Dod, 1996: The EDOP Radar System on the High-Altitude NASA ER-2 Aircraft, *J. Atmos. Oceanic Technol.,* 13, 795-809.

5. R. Meneghini and T. Kozu, Spaceborne Weather Radar, Artech House Ed., 1990, ISBN 0-89006-382-6
6. P. Amayenc et al. Proposal for a spaceborne dual-beam rain Radar with Doppler capability, , J. Atmos. Oceanic Technol., 10, June 93, pp.262-276.
7 E. Im, S. Tanelli, D. Giuli, S. Durden, and L. Facheris, Spaceborne radar measurements of rainfall vertical velocity, SPIE Second International Asia-Pacific Symposium on Remote Sensing of the Atmosphere, Environment and Space, Sendai (Japan), 9-12 October 2000
8. R.J. Doviak and Zrnic D.S., Doppler radar and weather observations, Academic Press, 1984.
9. D. Atlas, R.C. Srivastava and R.S. Sekhon, Doppler Radar characteristics of precipitation at vertical incidence. Rev. Geophys. Space Phys. 2, pp.1-35, 1973.
10. D.S. Zrnic': Estimation of spectral moments for weather echoes, IEEE Trans. On Geosc. Electr., 4, Oct. 1979, pp.113-128.
11. Marshall J.S. and Hitschfeld W., Interpretation of the fluctuating Echo for randomly distributed scatterers. Part I, Can. J. Phys., 31, pp.962-995, 1953.
12. A.L. Pazmany, J.C. Galloway, J.B. Mead, I. Popstefanija, R.E. McIntosh and H.W. Bluestein: Polarization Diversity Pulse-Pair Technique for Millimeter-Wave Doppler Radar Measurements of Severe Storm Features. J. Atmos. Ocean. Technol., 16, 1999, pp. 1900-1910.
13 H. Sauvageot, F. Mesnard and R. S. Tenorio, 1999: The relation between the area-average rain rate and the raincell size distribution parameters. J. Atmos. Sci., 56, 57-70.
14 S. Tanelli, E. Im, S. Durden, L. Facheris, D. Giuli and E. Smith, Spaceborne radar measurements of vertical rainfall velocity: the non-uniform beam filling considerations, Proc. International Geoscience and Remote Sensing Symposium 2001, Sydney (Australia) (CD-ROM)
15 F.T. Ulaby, R.K.Moore and A.K.Fung, 1982, Microwave Remote Sensing, Vol II, Addison-Wesley, 457-1064.